

A CELL-CENTERED FINITE DIFFERENCE METHOD ON QUADRILATERALS

MARY F. WHEELER* AND IVAN YOTOV†

Abstract. We develop a cell-centered finite difference method for elliptic problems on curvilinear quadrilateral grids. The method is based on the lowest order Brezzi-Douglas-Marini (BDM) mixed finite element method. A quadrature rule gives a block-diagonal mass matrix and allows for local flux elimination. The method is motivated and closely related to the multipoint flux approximation (MPFA) method. An advantage of our method is that it has a variational formulation. As a result finite element techniques can be employed to analyze the algebraic system and the convergence properties. The method exhibits second order convergence of the scalar variable at the cell-centers and of the flux at the midpoints of the edges. It performs well on problems with rough grids and coefficients, which is illustrated by numerical experiments.

Key words. Mixed finite element, multipoint flux approximation, cell centered finite difference, tensor coefficient.

AMS(MOS) subject classifications. 65N06, 65N12, 65N15, 65N30, 76S05.

1. Introduction. Cell-centered finite difference (CCFD) methods have been widely used in flow in porous media modeling, especially in the petroleum industry [5]. They combine local mass conservation and accuracy for discontinuous coefficients with relatively easy, compared to finite element methods, implementation and computational efficiency. CCFD methods, however, have certain accuracy limitations on irregular grids.

A relationship between CCFD methods and mixed finite element (MFE) methods was established by Russell and Wheeler [17] for rectangular grids and diagonal tensor coefficients. They noted that a special quadrature rule diagonalizes the velocity mass matrix and the MFE method reduces to CCFD for the pressure. This relation was exploited by Weiser and Wheeler [21] to obtain optimal convergence and superconvergence for both pressure and velocity in CCFD methods on rectangular grids. These results were extended to full tensor coefficients and triangular and logically rectangular grids by Arbogast et al. in [4, 3] by introducing the expanded mixed finite element (EMFE) method (see also related results by Vassilevski et al. [19], Baranger et al. [6], and Micheletti et al. [15] for triangular grids and diagonal tensor coefficients).

*Institute for Computational Engineering and Sciences (ICES), Department of Aerospace Engineering & Engineering Mechanics, and Department of Petroleum and Geosystems Engineering, The University of Texas at Austin, Austin, TX 78712 (mfw@ices.utexas.edu). Partially supported by NSF grant DMS 0411413 and the DOE grant DE-FGO2-04ER25617.

†Department of Mathematics, University of Pittsburgh, Pittsburgh, PA 15260 (yotov@math.pitt.edu). Supported in part by the DOE grant DE-FG02-04ER25618, and by the NSF grants DMS 0107389 and DMS 0411694.

The EMFE method is superconvergent for smooth grids and coefficients, but loses accuracy near discontinuities. Pressure Lagrange multipliers can be introduced along discontinuous interfaces to recover higher order convergence [3], which, however, leads to a hybrid cell-centered – face-centered formulation. Two other closely related methods that handle accurately rough grids and coefficients are the control volume mixed finite element (CVMFE) method, see Cai et al. [9], and the mimetic finite difference (MFD) methods, see Hyman et al. [12]. Each of these, however, as in the case of MFE methods, leads to an algebraic saddle-point problem. The multipoint flux approximation (MPFA) method, see Aavatsmark et al. [2, 1] has been developed as a finite volume method and combines the advantages of the above mentioned methods, i.e., it is accurate for rough grids and coefficients and reduces to a cell-centered stencil for the pressures. However, due to its non-variational formulation, the theoretical understanding of its convergence properties is limited. Relationships between the above methods have been studied by Russell and Klausen in [13].

Our goal in this paper is to develop and analyze an accurate cell-centered finite difference method for elliptic problems with full discontinuous tensor coefficients on curved quadrilateral grids. We base our approach on a mixed finite element method that reduces to a cell-centered stencil for the pressures via a special quadrature rule and local velocity elimination. Motivated by the MPFA method [1] where sub-edge fluxes are introduced, we consider the lowest order Brezzi-Douglas-Marini BDM_1 mixed finite element method [7, 8]. The BDM_1 velocity space on quadrilaterals has two degrees of freedom per edge. A special quadrature rule is employed that for each corner couples only the four associated degrees of freedom. The CCFD method is obtained by inverting the block-diagonal velocity mass matrix.

We develop the method for a second order elliptic problem that models single phase flow in porous media. The problem can be written as a system of two first order equations

$$\mathbf{u} = -K\nabla p \quad \text{in } \Omega, \quad (1.1)$$

$$\nabla \cdot \mathbf{u} = f \quad \text{in } \Omega, \quad (1.2)$$

$$p = g \quad \text{on } \Gamma_D, \quad (1.3)$$

$$\mathbf{u} \cdot \mathbf{n} = 0 \quad \text{on } \Gamma_N, \quad (1.4)$$

where the domain $\Omega \subset \mathbf{R}^2$ has a boundary $\partial\Omega = \overline{\Gamma}_D \cup \overline{\Gamma}_N$, $\Gamma_D \cap \Gamma_N = \emptyset$, $\text{measure}(\Gamma_D) > 0$, \mathbf{n} is the outward unit normal on $\partial\Omega$, and K is a symmetric, uniformly positive definite tensor satisfying, for some $0 < k_0 \leq k_1 < \infty$,

$$k_0 \xi^T \xi \leq \xi^T K(x) \xi \leq k_1 \xi^T \xi \quad \forall x \in \Omega, \quad \forall \xi \in \mathbf{R}^2. \quad (1.5)$$

In the above equations p is the pressure, \mathbf{u} is the Darcy velocity, and K represents the permeability divided by the viscosity.

REMARK 1.1. The choice of homogeneous Neumann boundary conditions and the assumption $\text{measure}(\Gamma_D) > 0$ are made for the sake of simplicity of the presentation. Non-homogeneous and full Neumann boundary conditions can also be handled.

We will use the following standard notation. For a subdomain $G \subset \mathbf{R}^2$, the $L^2(G)$ inner product (or duality pairing) and norm are denoted $(\cdot, \cdot)_G$ and $\|\cdot\|_G$, respectively, for scalar and vector valued functions. The norms of the Sobolev spaces $W_\infty^k(G)$, $k \in \mathbf{R}$ are denoted $\|\cdot\|_{k, \infty, G}$. Let $\|\cdot\|_{k, G}$ be the norm of the Hilbert space $H^k(G)$. We omit G in the subscript if $G = \Omega$. For a section of the domain or an element boundary $S \subset \mathbf{R}^1$ we write $\langle \cdot, \cdot \rangle_S$ and $\|\cdot\|_S$ for the $L^2(S)$ inner product (or duality pairing) and norm, respectively. We will also make use of the space

$$H(\text{div}; \Omega) = \{\mathbf{v} \in (\mathbf{L}^2(\Omega))^2 : \nabla \cdot \mathbf{v} \in L^2(\Omega)\}$$

equipped with the norm

$$\|\mathbf{v}\|_{\text{div}} = (\|\mathbf{v}\|^2 + \|\nabla \cdot \mathbf{v}\|^2)^{1/2}.$$

The weak formulation of (1.1)–(1.4) is: find $\mathbf{u} \in \mathbf{V}$ and $p \in W$ such that

$$(K^{-1}\mathbf{u}, \mathbf{v}) = (p, \nabla \cdot \mathbf{v}) - \langle g, \mathbf{v} \cdot \mathbf{n} \rangle_{\Gamma_D}, \quad \mathbf{v} \in \mathbf{V}, \quad (1.6)$$

$$(\nabla \cdot \mathbf{u}, w) = (f, w), \quad w \in W, \quad (1.7)$$

where

$$\mathbf{V} = \{\mathbf{v} \in H(\text{div}; \Omega) : \mathbf{v} \cdot \mathbf{n} = 0 \text{ on } \Gamma_N\}, \quad W = L^2(\Omega).$$

It is well known [8, 16] that (1.6)–(1.7) has a unique solution.

The rest of the paper is organized as follows. The numerical method and its analysis are developed in Section 2 and Section 3, respectively. As part of the analysis we establish approximation properties for the BDM_1 velocity spaces on curved quadrilaterals. We prove that the method converges with rate $O(h)$ in the L^2 -norm for the pressure and the velocity and with rate $O(h^2)$ for the pressure at the cell centers. Numerical experiments confirming the theoretical results and comparisons with the EMFE method are presented in Section 4.

2. The numerical method.

2.1. Definition of the finite element partition. Let \mathcal{T}_h be a shape regular and quasiuniform [10] finite element partition of Ω , consisting of small curvilinear perturbations (to be made precise later) of convex quadrilaterals. If an element has curved edges, we refer to it as curved quadrilateral. We assume that for each element $E \in \mathcal{T}_h$ there exists a bijection mapping $F_E : \hat{E} \rightarrow E$ where \hat{E} is the reference unit square with vertices

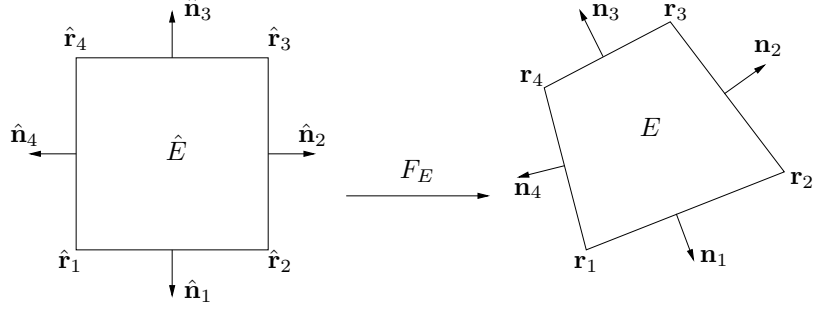


FIG. 1. Bilinear mapping and orientation of normal vectors.

$\hat{\mathbf{r}}_1 = (0, 0)^T$, $\hat{\mathbf{r}}_2 = (1, 0)^T$, $\hat{\mathbf{r}}_3 = (1, 1)^T$ and $\hat{\mathbf{r}}_4 = (0, 1)^T$. Denote by $\mathbf{r}_i = (x_i, y_i)^T$, $i = 1, \dots, 4$, the four corresponding vertices of element E as shown in Figure 1. The outward unit normal vectors to the edges of E and \hat{E} are denoted by \mathbf{n}_i and $\hat{\mathbf{n}}_i$, $i = 1, \dots, 4$, respectively. Let DF_E be the Jacobi matrix and let J_E be its Jacobian. We denote the inverse mapping by F_E^{-1} , its Jacobi matrix by DF_E^{-1} , and its Jacobian by $J_{F_E^{-1}}$. We have that

$$DF_E^{-1}(x) = (DF_E)^{-1}(\hat{x}), \quad J_{F_E^{-1}}(x) = \frac{1}{J_E(\hat{x})}.$$

It is easy to check that

$$\mathbf{n}_i = \frac{1}{J_{n_i}} J_E (DF_E^{-1})^T \hat{\mathbf{n}}_i, \quad \text{where } J_{n_i} = J_E |(DF_E^{-1})^T \hat{\mathbf{n}}_i|_{\mathbf{R}^2} \quad (2.1)$$

and $|\cdot|_{\mathbf{R}^2}$ is the Euclidean vector norm in \mathbf{R}^2 .

If E is a quadrilateral, then F_E is the bilinear mapping given by

$$\begin{aligned} F_E(\hat{\mathbf{r}}) &= \mathbf{r}_1 (1 - \hat{x})(1 - \hat{y}) + \mathbf{r}_2 \hat{x}(1 - \hat{y}) + \mathbf{r}_3 \hat{x}\hat{y} + \mathbf{r}_4 (1 - \hat{x})\hat{y} \\ &= \mathbf{r}_1 + \mathbf{r}_{21}\hat{x} + \mathbf{r}_{41}\hat{y} + (\mathbf{r}_{21} - \mathbf{r}_{34})\hat{x}\hat{y}, \end{aligned} \quad (2.2)$$

where $\mathbf{r}_{ij} = \mathbf{r}_i - \mathbf{r}_j$. In this case DF_E and J_E are linear functions of \hat{x} and \hat{y} :

$$\begin{aligned} DF_E &= [(1 - \hat{y}) \mathbf{r}_{21} + \hat{y} \mathbf{r}_{34}, (1 - \hat{x}) \mathbf{r}_{41} + \hat{x} \mathbf{r}_{32}] \\ &= [\mathbf{r}_{21}, \mathbf{r}_{41}] + [(\mathbf{r}_{21} - \mathbf{r}_{34})\hat{y}, (\mathbf{r}_{21} - \mathbf{r}_{34})\hat{x}], \end{aligned} \quad (2.3)$$

$$J_E = 2|T_1| + 2(|T_2| - |T_1|)\hat{x} + 2(|T_4| - |T_1|)\hat{y}, \quad (2.4)$$

where $|T_i|$ is the area of the triangle formed by the two edges sharing \mathbf{r}_i . Note that $J_E > 0$ for convex quadrilaterals. It is also easy to see that $J_{n_i} = |e_i|$ on any edge e_i .

If E is a curved quadrilateral, we assume that it is an $O(h^2)$ -perturbation of a quadrilateral, i.e.,

$$F_E = \tilde{F}_E + R(\hat{x}, \hat{y}), \quad \|R\|_{j, \infty, \hat{E}} \leq Ch^2, \quad j = 0, 1, 2, \quad (2.5)$$

where \tilde{F}_E is a bilinear map. We call such elements h^2 -quadrilaterals.

Let $a \sim b$ mean that there exist positive constants c_0 and c_1 independent of h such that $c_0 a \leq b \leq c_1 a$. For shape-regular and quasi-uniform quadrilateral grids, (2.3) and (2.4) imply that for all elements E

$$\|DF_E\|_{\infty, \hat{E}} \sim h, \quad \|J_E\|_{\infty, \hat{E}} \sim h^2, \quad \text{and} \quad \|J_{F_E^{-1}}\|_{\infty, \hat{E}} \sim h^{-2}. \quad (2.6)$$

Moreover, (2.6) also holds for any curved quadrilateral satisfying (2.5).

For the remainder of the paper we will restrict our attention to curved quadrilateral elements that are $O(h^2)$ -perturbations of parallelograms. We assume that

$$\|\mathbf{r}_{21} - \mathbf{r}_{34}\| \leq Ch^2. \quad (2.7)$$

Following the terminology adopted in [11], we call such elements h^2 -parallelograms.

REMARK 2.1. Note that the notion of h^2 -parallelograms from [11] is extended to elements with curved edges, i.e., elements that satisfy (2.5), where \tilde{F}_E satisfies (2.7).

Using (2.3), (2.5), and (2.7), a simple direct calculation shows that for h^2 -parallelograms

$$J_E = a + b(\hat{x}, \hat{y}) + d(\hat{x}, \hat{y}), \quad (2.8)$$

where $|a| \leq Ch^2$ is a constant, $|b(\hat{x}, \hat{y})| \leq Ch^3$ is a bilinear function, and $|d(\hat{x}, \hat{y})| \leq Ch^4$.

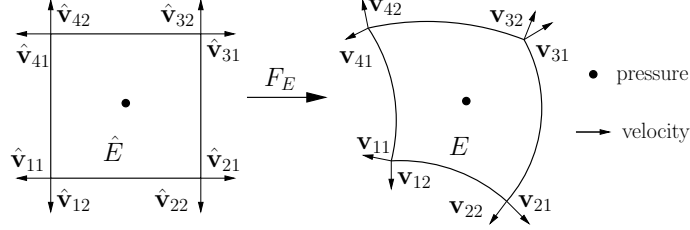
2.2. The BDM₁ spaces on curved quadrilaterals. Let $\mathbf{V}_h \times W_h$ be the lowest order BDM₁ mixed finite element spaces [7, 8]. On the reference unit square these spaces are defined as

$$\begin{aligned} \hat{\mathbf{V}}(\hat{E}) &= P_1(\hat{E})^2 + r \operatorname{curl}(\hat{x}^2 \hat{y}) + s \operatorname{curl}(\hat{x} \hat{y}^2) \\ &= \begin{pmatrix} \alpha_1 \hat{x} + \beta_1 \hat{y} + \gamma_1 + r \hat{x}^2 + 2s \hat{x} \hat{y} \\ \alpha_2 \hat{x} + \beta_2 \hat{y} + \gamma_2 - 2r \hat{x} \hat{y} - s \hat{y}^2 \end{pmatrix}, \end{aligned} \quad (2.9)$$

$$\hat{W}(\hat{E}) = P_0(\hat{E}) = \alpha,$$

where $\alpha, \alpha_1, \alpha_2, \beta_1, \beta_2, \gamma_1, \gamma_2, s, r$ are real constants and P_k denotes the space of polynomials of degree $\leq k$. Note that $\hat{\nabla} \cdot \hat{\mathbf{V}}(\hat{E}) = \hat{W}(\hat{E})$ and that for all $\hat{\mathbf{v}} \in \hat{\mathbf{V}}(\hat{E})$ and for any edge \hat{e} of \hat{E}

$$\hat{\mathbf{v}} \cdot \hat{\mathbf{n}}_{\hat{e}} \in P_1(\hat{e}).$$

FIG. 2. Degrees of freedom and basis functions for the BDM_1 spaces.

It is well known [7, 8] that the degrees of freedom for $\hat{\mathbf{V}}(\hat{E})$ can be chosen to be the values of $\hat{\mathbf{v}} \cdot \hat{\mathbf{n}}_{\hat{e}}$ at any two points on each edge \hat{e} . We choose these points to be the vertices of \hat{e} , see Figure 2. This choice is motivated by the requirement of accuracy and certain orthogonalities for the quadrature rule introduced in the next section.

The velocity space on any element E is defined via the Piola transformation

$$\mathbf{v} \leftrightarrow \hat{\mathbf{v}} : \quad \mathbf{v} = \frac{1}{J_E} DF_E \hat{\mathbf{v}} \circ F_E^{-1}$$

and the pressure space is defined via the standard change of variables

$$w \leftrightarrow \hat{w} : \quad w = \hat{w} \circ F_E^{-1}.$$

The BDM_1 spaces on \mathcal{T}_h are given by

$$\begin{aligned} \mathbf{V}_h &= \{ \mathbf{v} \in \mathbf{V} : \quad \mathbf{v}|_E \leftrightarrow \hat{\mathbf{v}}, \hat{\mathbf{v}} \in \hat{\mathbf{V}}(\hat{E}) \quad \forall E \in \mathcal{T}_h \}, \\ W_h &= \{ w \in W : \quad w|_E \leftrightarrow \hat{w}, \hat{w} \in \hat{W}(\hat{E}) \quad \forall E \in \mathcal{T}_h \}. \end{aligned} \quad (2.10)$$

The Piola transformation preserves the normal components of the velocity vectors on the edges and satisfies [8]

$$(\nabla \cdot \mathbf{v}, w)_E = (\hat{\nabla} \cdot \hat{\mathbf{v}}, \hat{w})_{\hat{E}} \quad \text{and} \quad \langle \mathbf{v} \cdot \mathbf{n}_i, w \rangle_{e_i} = \langle \hat{\mathbf{v}} \cdot \hat{\mathbf{n}}_i, \hat{w} \rangle_{\hat{e}_i}. \quad (2.11)$$

Moreover, (2.1) implies

$$\mathbf{v} \cdot \mathbf{n}_i = \frac{1}{J_E} DF_E \hat{\mathbf{v}} \cdot \frac{1}{J_{n_i}} J_E (DF_E^{-1})^T \hat{\mathbf{n}}_i = \frac{1}{J_{n_i}} \hat{\mathbf{v}} \cdot \hat{\mathbf{n}}_i. \quad (2.12)$$

Let $\hat{\Pi} : (H^1(\hat{E}))^2 \rightarrow \hat{\mathbf{V}}(\hat{E})$ be the reference element projection operator satisfying

$$\forall \hat{e}_i \subset \partial \hat{E}, \quad \langle (\hat{\Pi} \hat{\mathbf{q}} - \hat{\mathbf{q}}) \cdot \hat{\mathbf{n}}_i, \hat{p}_1 \rangle_{\hat{e}_i} = 0 \quad \forall \hat{p}_1 \in P_1(\hat{e}_i). \quad (2.13)$$

The divergence theorem and (2.13) imply that

$$(\hat{\nabla} \cdot (\hat{\Pi} \hat{\mathbf{q}} - \hat{\mathbf{q}}), \hat{w})_{\hat{E}} = 0 \quad \forall \hat{w} \in \hat{W}(\hat{E}). \quad (2.14)$$

Following [18, 20, 3], the operator Π is defined locally on each element E by

$$\Pi \mathbf{q} \leftrightarrow \widehat{\Pi \mathbf{q}}, \quad \widehat{\Pi \mathbf{q}} := \widehat{\Pi} \widehat{\mathbf{q}} \quad \forall \mathbf{q} \in (H^1(E))^2. \quad (2.15)$$

It is shown in [20] that in the case of quadrilaterals Π is a well defined operator from $\mathbf{V} \cap (H^1(\Omega))^d$ onto \mathbf{V}_h satisfying

$$(\nabla \cdot (\Pi \mathbf{q} - \mathbf{q}), w) = 0 \quad \forall w \in W_h \quad (2.16)$$

and

$$\|\Pi \mathbf{q}\|_{\text{div}} \leq C \|\mathbf{q}\|_1. \quad (2.17)$$

Due to (2.11), property (2.16) extends trivially to the case of curved quadrilaterals. The continuity bound (2.17) follows from the argument for proving the approximation properties of Π , which is given in Lemma A.1 in the Appendix.

Using an argument due to Fortin (see [8]) and properties (2.16)–(2.17), it can be shown that the BDM₁ spaces on curved quadrilaterals satisfy the inf-sup condition

$$\inf_{\substack{w \in W_h \\ w \neq 0}} \sup_{\substack{\mathbf{v} \in \mathbf{V}_h \\ \mathbf{v} \neq 0}} \frac{(\nabla \cdot \mathbf{v}, w)}{\|\mathbf{v}\|_{\text{div}} \|w\|} \geq \beta, \quad (2.18)$$

where β is a positive constant independent of h .

The following auxiliary estimate will be used in the analysis of the method.

LEMMA 2.1. *If $E \in \mathcal{T}_h$ and $\mathbf{q} \in (L^2(E))^2$, then*

$$\|\mathbf{q}\|_E \sim \|\widehat{\mathbf{q}}\|_{\widehat{E}}. \quad (2.19)$$

Proof. The statement of the lemma follows immediately from the relations

$$\begin{aligned} \int_E \mathbf{q} \cdot \mathbf{q} \, d\mathbf{x} &= \int_{\widehat{E}} \frac{1}{J_E} DF_E \widehat{\mathbf{q}} \cdot \frac{1}{J_E} DF_E \widehat{\mathbf{q}} J_E \, d\widehat{\mathbf{x}}, \\ \int_{\widehat{E}} \widehat{\mathbf{q}} \cdot \widehat{\mathbf{q}} \, d\widehat{\mathbf{x}} &= \int_E \frac{1}{J_{F_E^{-1}}} DF_E^{-1} \mathbf{q} \cdot \frac{1}{J_{F_E^{-1}}} DF_E^{-1} \mathbf{q} J_{F_E^{-1}} \, d\mathbf{x}, \end{aligned}$$

and bounds(2.6). \square

The BDM₁ mixed finite element method is based on approximating the variational formulation (1.6)–(1.7) in the discrete spaces $\mathbf{V}_h \times W_h$: find $\mathbf{u}_h^{bdm} \in \mathbf{V}_h$ and $p_h^{bdm} \in W_h$ such that

$$(K^{-1} \mathbf{u}_h^{bdm}, \mathbf{v}) = (p_h^{bdm}, \nabla \cdot \mathbf{v}) - \langle g, \mathbf{v} \cdot \mathbf{n} \rangle_{\Gamma_D}, \quad \mathbf{v} \in \mathbf{V}_h, \quad (2.20)$$

$$(\nabla \cdot \mathbf{u}_h^{bdm}, w) = (f, w), \quad w \in W_h. \quad (2.21)$$

It has been shown in [20] that on quadrilaterals the above method has a unique solution and that it is second order accurate for the velocity and first order accurate for the pressure in the L^2 -norm. These results can be extended to h^2 -quadrilaterals in light of the approximation results of Lemma A.1. The method handles well discontinuous coefficients due to the presence of K^{-1} in the mass matrix. However, the resulting algebraic system is a coupled velocity-pressure system and it can be quite large. Moreover, it is of a saddle-point problem type. Our goal is to design a quadrature rule that allows for local elimination of the velocities and results in a positive definite cell-centered pressure matrix.

2.3. A quadrature rule. For $\mathbf{q}, \mathbf{v} \in \mathbf{V}_h$, define the global quadrature rule

$$(K^{-1}\mathbf{q}, \mathbf{v})_Q \equiv \sum_{E \in \mathcal{T}_h} (K^{-1}\mathbf{q}, \mathbf{v})_{Q,E}.$$

The integration on any element E is performed by mapping to the reference element \hat{E} . The quadrature rule is defined on \hat{E} . Using the definition (2.10) of the finite element spaces we have

$$\begin{aligned} \int_E K^{-1}\mathbf{q} \cdot \mathbf{v} \, d\mathbf{x} &= \int_{\hat{E}} \hat{K}^{-1} \frac{1}{J_E} DF_E \hat{\mathbf{q}} \cdot \frac{1}{J_E} DF_E \hat{\mathbf{v}} J_E \, d\hat{\mathbf{x}} \\ &= \int_{\hat{E}} \frac{1}{J_E} DF_E^T \hat{K}^{-1} DF_E \hat{\mathbf{q}} \cdot \hat{\mathbf{v}} \, d\hat{\mathbf{x}} \equiv \int_{\hat{E}} \mathcal{K}^{-1} \hat{\mathbf{q}} \cdot \hat{\mathbf{v}} \, d\hat{\mathbf{x}}, \end{aligned}$$

where

$$\mathcal{K} = J_E DF_E^{-1} \hat{K} (DF_E^{-1})^T. \quad (2.22)$$

It is easy to see that bounds (2.6) imply

$$\|\mathcal{K}\|_{\infty, \hat{E}} \sim \|K\|_{\infty, E} \quad \text{and} \quad \|\mathcal{K}^{-1}\|_{\infty, \hat{E}} \sim \|K^{-1}\|_{\infty, E}. \quad (2.23)$$

The quadrature rule on an element E is defined as

$$(K^{-1}\mathbf{q}, \mathbf{v})_{Q,E} \equiv (\mathcal{K}^{-1} \hat{\mathbf{q}}, \hat{\mathbf{v}})_{\hat{Q}, \hat{E}} \equiv \frac{|\hat{E}|}{4} \sum_{i=1}^4 \mathcal{K}^{-1}(\hat{\mathbf{r}}_i) \hat{\mathbf{q}}(\hat{\mathbf{r}}_i) \cdot \hat{\mathbf{v}}(\hat{\mathbf{r}}_i). \quad (2.24)$$

Note that on \hat{E} this is the trapezoidal quadrature rule.

The corner vector $\hat{\mathbf{q}}(\hat{\mathbf{r}}_i)$ is uniquely determined by its normal components to the two edges that share that vertex. Recall that we chose the velocity degrees of freedom on any edge \hat{e} to be the normal components at the vertices of \hat{e} . Therefore, there are two degrees of freedom associated with each corner $\hat{\mathbf{r}}_i$ and they uniquely determine the corner vector $\hat{\mathbf{q}}(\hat{\mathbf{r}}_i)$. More precisely,

$$\hat{\mathbf{q}}(\hat{\mathbf{r}}_i) = \sum_{j=1}^2 (\hat{\mathbf{q}} \cdot \hat{\mathbf{n}}_{ij})(\hat{\mathbf{r}}_i) \hat{\mathbf{n}}_{ij},$$

where $\hat{\mathbf{n}}_{ij}$, $j = 1, 2$, are the outward unit normal vectors to the two edges intersecting at $\hat{\mathbf{r}}_i$, and $(\hat{\mathbf{q}} \cdot \hat{\mathbf{n}}_{ij})(\hat{\mathbf{r}}_i)$ are the velocity degrees of freedom associated with this corner. Let us denote the basis functions associated with $\hat{\mathbf{r}}_i$ by $\hat{\mathbf{v}}_{ij}$, $j = 1, 2$ (see Figure 2), i.e.,

$$\begin{aligned} (\hat{\mathbf{v}}_{ij} \cdot \hat{\mathbf{n}}_{ij})(\hat{\mathbf{r}}_i) &= 1, & (\hat{\mathbf{v}}_{ij} \cdot \hat{\mathbf{n}}_{lk})(\hat{\mathbf{r}}_i) &= 0, & k \neq j, \text{ and} \\ (\hat{\mathbf{v}}_{ij} \cdot \hat{\mathbf{n}}_{lk})(\hat{\mathbf{r}}_l) &= 0, & l \neq i, k &= 1, 2. \end{aligned}$$

Clearly the quadrature rule (2.24) only couples the two basis functions associated with a corner. For example,

$$(\mathcal{K}^{-1}\hat{\mathbf{v}}_{11}, \hat{\mathbf{v}}_{11})_{\hat{Q}, \hat{E}} = \frac{\mathcal{K}_{22}^{-1}(\hat{\mathbf{r}}_1)}{4}, \quad (\mathcal{K}^{-1}\hat{\mathbf{v}}_{11}, \hat{\mathbf{v}}_{12})_{\hat{Q}, \hat{E}} = \frac{\mathcal{K}_{12}^{-1}(\hat{\mathbf{r}}_1)}{4}, \quad (2.25)$$

and

$$(\mathcal{K}^{-1}\hat{\mathbf{v}}_{11}, \hat{\mathbf{v}}_{ij})_{\hat{Q}, \hat{E}} = 0 \quad \forall ij \neq 11, 12. \quad (2.26)$$

REMARK 2.2. On quadrilaterals the quadrature rule can be defined directly on an element E . It is easy to see from (2.4) that

$$(K^{-1}\mathbf{q}, \mathbf{v})_{Q, E} = \frac{1}{2} \sum_{i=1}^4 |T_i| K^{-1}(\mathbf{r}_i) \mathbf{q}(\mathbf{r}_i) \cdot \mathbf{v}(\mathbf{r}_i). \quad (2.27)$$

The above quadrature rule is closely related to an inner product used in the mimetic finite difference methods [12]. We note that it is simpler to evaluate the quadrature rule on the reference element \hat{E} .

Denote the element quadrature error by

$$\sigma_E(K^{-1}\mathbf{q}, \mathbf{v}) \equiv (K^{-1}\mathbf{q}, \mathbf{v})_E - (K^{-1}\mathbf{q}, \mathbf{v})_{Q, E} \quad (2.28)$$

and define the global quadrature error by $\sigma(K^{-1}\mathbf{q}, \mathbf{v})|_E = \sigma_E(K^{-1}\mathbf{q}, \mathbf{v})$.

2.4. The multipoint flux mixed finite element method. We are now ready to define our method. We seek $\mathbf{u}_h \in \mathbf{V}_h$ and $p_h \in W_h$ such that

$$(K^{-1}\mathbf{u}_h, \mathbf{v})_Q = (p_h, \nabla \cdot \mathbf{v}) - \langle g, \mathbf{v} \cdot \mathbf{n} \rangle_{\Gamma_D}, \quad \mathbf{v} \in \mathbf{V}_h, \quad (2.29)$$

$$(\nabla \cdot \mathbf{u}_h, w) = (f, w), \quad w \in W_h. \quad (2.30)$$

REMARK 2.3. We call the method (2.29)–(2.30) a multipoint flux mixed finite element (MFMFE) method due to its relation to the MPFA method.

To establish solvability of (2.29)–(2.30) we need the following coercivity result.

LEMMA 2.2. *There exists a constant C independent of h such that*

$$(K^{-1}\mathbf{q}, \mathbf{q})_Q \geq C \|\mathbf{q}\|^2 \quad \forall \mathbf{q} \in \mathbf{V}_h. \quad (2.31)$$

Proof. Let $\mathbf{q} \leftrightarrow \hat{\mathbf{q}}$ and $\hat{\mathbf{q}} = \sum_{i=1}^4 \sum_{j=1}^2 \hat{q}_{ij} \hat{\mathbf{v}}_{ij}$. We have

$$\begin{aligned} (K^{-1}\mathbf{q}, \mathbf{q})_{Q,E} &= \frac{|\hat{E}|}{4} \sum_{i=1}^4 \mathcal{K}^{-1}(\hat{\mathbf{r}}_i) \hat{\mathbf{q}}(\hat{\mathbf{r}}_i) \cdot \hat{\mathbf{q}}(\hat{\mathbf{r}}_i) \\ &\geq \frac{C}{k_1} \sum_{i=1}^4 \hat{\mathbf{q}}(\hat{\mathbf{r}}_i) \cdot \hat{\mathbf{q}}(\hat{\mathbf{r}}_i) = \frac{C}{k_1} \sum_{i=1}^4 \sum_{j=1}^2 \hat{q}_{ij}^2, \end{aligned}$$

where we used (2.23) and (1.5) in the inequality, and the location of the degrees of freedom at the vertices in the last equality. On the other hand, using (2.19),

$$\|\mathbf{q}\|_E^2 \leq C(\hat{\mathbf{q}}, \hat{\mathbf{q}})_{\hat{E}} = C \left(\sum_{i=1}^4 \sum_{j=1}^2 \hat{q}_{ij} \hat{\mathbf{v}}_{ij}, \sum_{k=1}^4 \sum_{l=1}^2 \hat{q}_{kl} \hat{\mathbf{v}}_{kl} \right) \leq C \sum_{i=1}^4 \sum_{j=1}^2 \hat{q}_{ij}^2.$$

The assertion of the lemma follows from the above two estimates. \square

REMARK 2.4. Lemma 2.2 implies that $(K^{-1}\cdot, \cdot)_Q^{1/2}$ is a norm in \mathbf{V}_h . Let us denote this norm by $\|\cdot\|_Q$. It is easy to see that $\|\cdot\|_Q$ is equivalent to $\|\cdot\|$. Indeed, using (2.23), (1.5), the equivalence of norms on reference element \hat{E} , and (2.19), we have that for all $\mathbf{q} \in \mathbf{V}_h$

$$(K^{-1}\mathbf{q}, \mathbf{q})_{Q,E} = (\mathcal{K}^{-1}\hat{\mathbf{q}}, \hat{\mathbf{q}})_{\hat{Q},\hat{E}} \leq \frac{C}{k_0} \|\hat{\mathbf{q}}\|_{\hat{E}}^2 \leq C \|\mathbf{q}\|_E^2,$$

which, combined with (2.31), implies that

$$c_0 \|\mathbf{q}\| \leq \|\mathbf{q}\|_Q \leq c_1 \|\mathbf{q}\| \quad (2.32)$$

for some positive constants c_0 and c_1 .

LEMMA 2.3. *The multipoint flux mixed finite element method (2.29)–(2.30) has a unique solution.*

Proof. Since (2.29)–(2.30) is a square system, it is enough to show uniqueness. Letting $f = 0$ and $g = 0$ and taking $\mathbf{v} = \mathbf{u}_h$ and $w = p_h$, we conclude that $(K^{-1}\mathbf{u}_h, \mathbf{u}_h)_Q = 0$, and therefore $\mathbf{u}_h = 0$, due to (2.31). Let ϕ be the solution to

$$\begin{aligned} -\nabla \cdot K \nabla \phi &= -p_h && \text{in } \Omega, \\ \phi &= 0 && \text{on } \Gamma_D, \\ -K \nabla \phi \cdot \mathbf{n} &= 0 && \text{on } \Gamma_N. \end{aligned}$$

Taking $\mathbf{v} = \Pi K \nabla \phi \in \mathbf{V}_h$ in (2.29) and using (2.16), we obtain

$$0 = (p_h, \nabla \cdot \Pi K \nabla \phi) = (p_h, \nabla \cdot K \nabla \phi) = \|p_h\|^2,$$

implying $p_h = 0$. \square

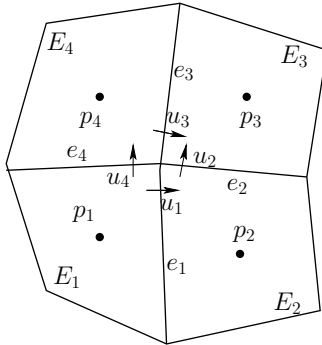


FIG. 3. Four elements sharing a vertex.

2.5. Reduction to a cell-centered finite difference method.

The multipoint flux mixed finite element method presented above reduces to a cell-centered system for the pressures. Let us consider any interior vertex \mathbf{r} and suppose that it is shared by elements E_1, \dots, E_4 , see Figure 3. We denote the edges that share the vertex by e_1, \dots, e_4 , the velocity basis functions on these edges that are associated with the vertex by $\mathbf{v}_1, \dots, \mathbf{v}_4$, and the corresponding values of the normal components of \mathbf{u}_h by u_1, \dots, u_4 . Note that for clarity the normal velocities on Figure 3 are drawn at a distance from the vertex.

Due to the locality of the basis functions interaction in the quadrature rule $(K^{-1}\cdot, \cdot)_Q$ in (2.25)–(2.26), taking, for example, $\mathbf{v} = \mathbf{v}_1$ in (2.29) will only lead to coupling u_1 with u_4 and u_2 . Therefore, the four equations obtained from taking $\mathbf{v} = \mathbf{v}_1, \dots, \mathbf{v}_4$ form a linear system for u_1, \dots, u_4 . Note that the coefficients of this linear system are

$$a_{ij} = (K^{-1}\mathbf{v}_i, \mathbf{v}_j)_Q, \quad i, j = 1, \dots, 4.$$

The local linear system is symmetric and, due to (2.31), positive definite, and it is therefore invertible. Solving the 4×4 linear system allows to express the velocities u_i in terms of the cell-centered pressures p_i , $i = 1, \dots, 4$. Substituting these expressions into the mass conservation equation (2.30) leads to a cell-centered stencil. The pressure in each element E is coupled with the pressures in the elements that share a vertex with E . On logically rectangular grids this is a 9-point stencil.

We give the equation obtained by taking $\mathbf{v} = \mathbf{v}_1$ in (2.29). On the left hand side we have

$$(K^{-1}\mathbf{u}_h, \mathbf{v}_1)_Q = (K^{-1}\mathbf{u}_h, \mathbf{v}_1)_{Q, E_1} + (K^{-1}\mathbf{u}_h, \mathbf{v}_1)_{Q, E_2}. \quad (2.33)$$

The first term on the right above gives

$$\begin{aligned}
(K^{-1}\mathbf{u}_h, \mathbf{v}_1)_{Q, E_1} &= (\mathcal{K}^{-1}\hat{\mathbf{u}}_h, \hat{\mathbf{v}}_1)_{\hat{Q}, \hat{E}} \\
&= \frac{1}{4}(\mathcal{K}_{11, E_1}^{-1}\hat{u}_1\hat{v}_{1,1} + \mathcal{K}_{12, E_1}^{-1}\hat{u}_4\hat{v}_{1,1}) \\
&= \frac{1}{4}(\mathcal{K}_{11, E_1}^{-1}J_{n_1}u_1 + \mathcal{K}_{12, E_1}^{-1}J_{n_4}u_4)J_{n_1},
\end{aligned} \tag{2.34}$$

where we have used (2.12) for the last equality. Here $\mathcal{K}_{ij, E_1}^{-1}$ denotes a component of \mathcal{K}^{-1} in E_1 and all functions are evaluated at the vertex $\hat{\mathbf{r}}_3$ of \hat{E} , the vertex corresponding to vertex \mathbf{r} in the mapping F_{E_1} . Similarly,

$$(K^{-1}\mathbf{u}_h, \mathbf{v}_1)_{Q, E_1} = \frac{1}{4}(\mathcal{K}_{11, E_2}^{-1}J_{n_1}u_1 + \mathcal{K}_{12, E_2}^{-1}J_{n_2}u_2)J_{n_1}. \tag{2.35}$$

For the right hand side of (2.29) we write

$$\begin{aligned}
(p_h, \nabla \cdot \mathbf{v}_1) &= (p_h, \nabla \cdot \mathbf{v}_1)_{E_1} + (p_h, \nabla \cdot \mathbf{v}_1)_{E_2} \\
&= \langle p_h, \mathbf{v}_1 \cdot \mathbf{n}_{E_1} \rangle_{e_1} + \langle p_h, \mathbf{v}_1 \cdot \mathbf{n}_{E_2} \rangle_{e_1} \\
&= \langle \hat{p}_h, \hat{\mathbf{v}}_1 \cdot \hat{\mathbf{n}}_{E_1} \rangle_{\hat{e}_1} + \langle \hat{p}_h, \hat{\mathbf{v}}_1 \cdot \hat{\mathbf{n}}_{E_2} \rangle_{\hat{e}_1} \\
&= \frac{1}{2}(p_1 - p_2)J_{n_1},
\end{aligned} \tag{2.36}$$

where we have used the trapezoidal rule for the integrals on \hat{e}_1 , which is exact since \hat{p}_h is constant and $\hat{\mathbf{v}}_1 \cdot \hat{\mathbf{n}}$ is linear. A combination of (2.33)–(2.36) gives the equation

$$\frac{1}{2}((\mathcal{K}_{11, E_1}^{-1} + \mathcal{K}_{11, E_2}^{-1})J_{n_1}u_1 + \mathcal{K}_{12, E_1}^{-1}J_{n_4}u_4 + \mathcal{K}_{12, E_2}^{-1}J_{n_2}u_2) = p_1 - p_2.$$

The other three equations of the local system for u_1, \dots, u_4 are obtained similarly.

REMARK 2.5. The above construction is also valid for vertices on the boundary $\partial\Omega$. In the case of Dirichlet boundary conditions, a 3×3 system allows to express the velocities in terms of cell and boundary pressures. In the case of Neumann boundary conditions, the one unknown vertex velocity is expressed in terms of the two cell pressures and two boundary fluxes.

3. Error analysis. We will make use of the L^2 -orthogonal projection onto W_h . For any $\phi \in L^2(\Omega)$, let $\mathcal{Q}_h\phi \in W_h$ be its $L^2(\Omega)$ projection satisfying

$$(\phi - \mathcal{Q}_h\phi, w) = 0 \quad \forall w \in W_h.$$

It is well known [10] that the L^2 -projection has the approximation property

$$\|\phi - \mathcal{Q}_h\phi\| \leq C\|\phi\|_r h^r, \quad 0 \leq r \leq 1. \tag{3.1}$$

The convergence analysis of the method (2.29)–(2.30) is similar to the analysis in the case of straight edge quadrilaterals presented in [22]. The following estimates hold.

THEOREM 3.1. *If $K^{-1} \in W^{1,\infty}(E)$ for all elements E , then there exists a constant C independent of h such that*

$$\|\mathbf{u} - \mathbf{u}_h\| \leq Ch\|\mathbf{u}\|_1, \quad (3.2)$$

$$\|\nabla \cdot (\mathbf{u} - \mathbf{u}_h)\| \leq Ch\|\nabla \cdot \mathbf{u}\|_1, \quad (3.3)$$

$$\|p - p_h\| \leq Ch(\|\mathbf{u}\|_1 + \|p\|_1). \quad (3.4)$$

Moreover, if the problem (1.1)–(1.4) has H^2 -elliptic regularity, and if $K \in W^{1,\infty}(E)$ and $K^{-1} \in W^{2,\infty}(E)$ for all elements E , then

$$\|\mathcal{Q}_h p - p_h\| \leq Ch^2(\|\mathbf{u}\|_1 + \|\nabla \cdot \mathbf{u}\|_1). \quad (3.5)$$

The proof of the theorem uses the following bounds on the quadrature error.

LEMMA 3.1. *If $K^{-1} \in W^{1,\infty}(E)$ for all elements E , then there exists a constant C independent of h such that for all $\mathbf{v} \in \mathbf{V}_h$*

$$|\sigma(K^{-1}\Pi\mathbf{u}, \mathbf{v})| \leq Ch\|\mathbf{u}\|_1\|\mathbf{v}\|. \quad (3.6)$$

If $K^{-1} \in W^{2,\infty}(E)$ for all elements E , then, for all $\mathbf{v}, \mathbf{q} \in \mathbf{V}_h$,

$$|\sigma(K^{-1}\mathbf{q}, \mathbf{v})| \leq C \sum_{E \in \mathcal{T}_h} h^2 \|\mathbf{q}\|_{1,E} \|\mathbf{v}\|_{1,E}. \quad (3.7)$$

The proof of the above lemma follows closely the argument presented in [22] for straight-edge quadrilaterals. The error on any element E is bounded through mapping to the reference element \hat{E} , employing bounds on the trapezoidal quadrature error, and mapping back to E . We refer the reader to [22] for details.

Proof of Theorem 3.1. Subtracting the numerical scheme (2.29)–(2.30) from the variational formulation (1.6)–(1.7) gives the error equations

$$\begin{aligned} (K^{-1}(\Pi\mathbf{u} - \mathbf{u}_h), \mathbf{v})_Q &= (Q_h p - p_h, \nabla \cdot \mathbf{v}) + (K^{-1}(\Pi\mathbf{u} - \mathbf{u}), \mathbf{v}) \\ &\quad - \sigma(K^{-1}\Pi\mathbf{u}, \mathbf{v}), \quad \mathbf{v} \in \mathbf{V}_h, \end{aligned} \quad (3.8)$$

$$(\nabla \cdot (\Pi\mathbf{u} - \mathbf{u}_h), w) = 0, \quad w \in W_h. \quad (3.9)$$

First note that (A.6) implies that on any element E we can choose $w = J_E \nabla \cdot (\Pi\mathbf{u} - \mathbf{u}_h) \in W_h$ in (3.9). Since J_E is uniformly positive, this implies that

$$\nabla \cdot (\Pi\mathbf{u} - \mathbf{u}_h) = 0. \quad (3.10)$$

Bound (3.3) follows from (3.10) and (A.3).

To show (3.2), take $\mathbf{v} = \Pi\mathbf{u} - \mathbf{u}_h$ in (3.9) to obtain

$$(K^{-1}(\Pi\mathbf{u} - \mathbf{u}_h), \Pi\mathbf{u} - \mathbf{u}_h)_Q = (K^{-1}(\Pi\mathbf{u} - \mathbf{u}), \Pi\mathbf{u} - \mathbf{u}_h) - \sigma(K^{-1}\Pi\mathbf{u}, \Pi\mathbf{u} - \mathbf{u}_h). \quad (3.11)$$

Using (A.1), the first term on the right above is bounded by

$$|(K^{-1}(\Pi\mathbf{u} - \mathbf{u}), \Pi\mathbf{u} - \mathbf{u}_h)| \leq Ch\|\mathbf{u}\|_1\|\Pi\mathbf{u} - \mathbf{u}_h\|. \quad (3.12)$$

The second term on the right in (3.11) can be bounded using Lemma 3.1,

$$|\sigma(K^{-1}\Pi\mathbf{u}, \Pi\mathbf{u} - \mathbf{u}_h)| \leq Ch\|\mathbf{u}\|_1\|\Pi\mathbf{u} - \mathbf{u}_h\|. \quad (3.13)$$

A combination of (3.11), (3.12), (3.13), (2.31), and (A.1) completes the proof of (3.2).

Using the inf-sup condition (2.18) and (3.9), we obtain

$$\begin{aligned} & \|\mathcal{Q}_h p - p_h\| \\ & \leq \frac{1}{\beta} \sup_{\substack{\mathbf{v} \in \mathbf{V}_h \\ \mathbf{v} \neq 0}} \frac{(\nabla \cdot \mathbf{v}, \mathcal{Q}_h p - p_h)}{\|\mathbf{v}\|_{\text{div}}} \\ & = \frac{1}{\beta} \sup_{\substack{\mathbf{v} \in \mathbf{V}_h \\ \mathbf{v} \neq 0}} \frac{(K^{-1}(\Pi\mathbf{u} - \mathbf{u}_h), \mathbf{v})_Q - (K^{-1}(\Pi\mathbf{u} - \mathbf{u}), \mathbf{v}) + \sigma(K^{-1}\Pi\mathbf{u}, \mathbf{v})}{\|\mathbf{v}\|_{\text{div}}} \\ & \leq \frac{C}{\beta} h\|\mathbf{u}\|_1, \end{aligned}$$

where we have used the Cauchy-Schwarz inequality, (3.2), (A.1), and (3.6) in the last inequality. The proof of (3.4) is completed by an application of the triangle inequality and (3.1).

The proof of (3.5) is based on a duality argument and employs the quadrature error bound (3.7); see [22] for details. \square

4. Numerical experiments. In this section we present several numerical experiments that confirm the theoretical results of the previous section. In the first example we take $K = 2 * I$ and solve a problem with Neumann boundary conditions and a known solution

$$p(x, y) = \cos(2\pi(x + 1/2)) \cos(2\pi(y + 1/2)).$$

The domain has an irregular shape, see Figure 4. It is partitioned by curved quadrilaterals. Note that the numerical grid is smooth, except across the vertical line that cuts through the middle. Due to (2.22), the non-smoothness of the grid translates into a discontinuous computational permeability \mathcal{K} . We test the convergence of our method on a sequence of

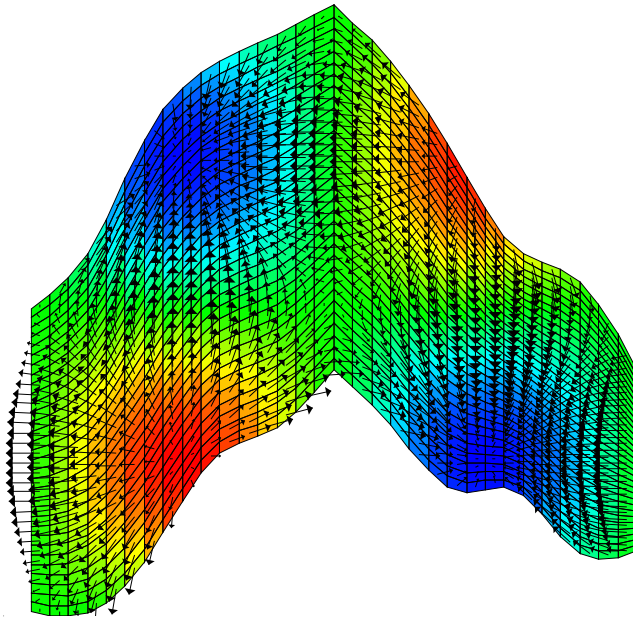


FIG. 4. Computed pressure (color) and velocity (arrows) with the MFME method in Example 1.

six meshes, from 8×8 to 256×256 . The computed solution on the 32×32 mesh is shown in Figure 4. The MFME method is compared to the EMFE method of [4, 3]. The two methods have comparable computational costs, as each one reduces to CCFD for the pressure. The discretization errors and asymptotic convergence rates are presented in Table 1. Here $|||p - p_h|||$ denotes a discrete pressure L^2 -norm that involves only the function values at the cell-centers and $|||\mathbf{u} - \mathbf{u}_h|||$ denotes a discrete velocity L^2 -norm that involves only the normal vector components at the midpoints of the edges. We note that for the MFME method the obtained convergence rates of $O(h^2)$ for $|||p - p_h|||$ and $O(h)$ for $|||\mathbf{u} - \mathbf{u}_h|||$ confirm the theoretical results. The $O(h^2)$ accuracy for $|||\mathbf{u} - \mathbf{u}_h|||$ indicates superconvergence for the normal velocities at the midpoints of the edges. At the same time, the EMFE method exhibits only $O(h)$ convergence for the pressure and $O(h^{1/2})$ for the velocity. The slower convergence is due to reduced accuracy along the discontinuity, as it can be seen in Figure 5.

In the second example we test our method on a sequence of meshes obtained by a uniform refinement of an initial rough quadrilateral mesh. It is easy to see that the resulting partitions consist of h^2 -parallelograms. We take $K = 2 * I$, Dirichlet boundary conditions, and a true solution

$$p(x, y) = x^3y + y^4 + \sin(x) \cos(y).$$

TABLE 1
Discretization errors and convergence rates for Example 1.

	MFMFE method			EMFE method	
$1/h$	$\ p - p_h\ $	$\ \mathbf{u} - \mathbf{u}_h\ $	$\ \mathbf{u} - \mathbf{u}_h\ $	$\ p - p_h\ $	$\ \mathbf{u} - \mathbf{u}_h\ $
8	0.17E0	0.37E0	0.17E0	0.21E+1	0.37E0
16	0.60E-1	0.21E0	0.46E-1	0.26E0	0.24E0
32	0.97E-2	0.11E0	0.12E-1	0.74E-1	0.16E0
64	0.25E-2	0.58E-1	0.29E-2	0.31E-1	0.12E0
128	0.67E-3	0.29E-1	0.72E-3	0.14E-1	0.84E-1
256	0.17E-3	0.15E-1	0.18E-3	0.70E-2	0.60E-1
Rate	1.99	0.99	2.00	1.04	0.48

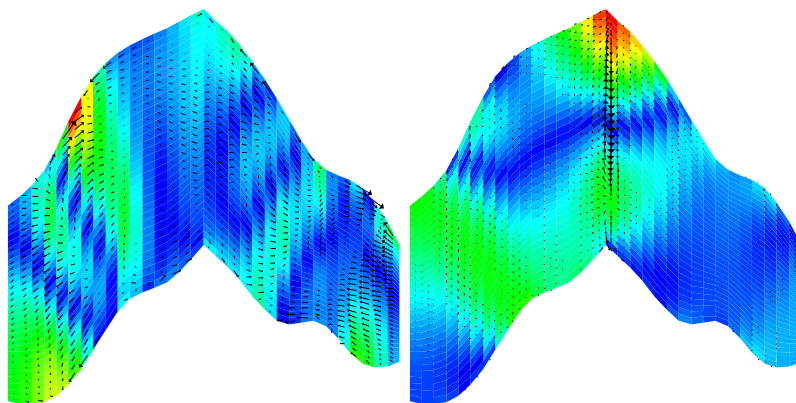


FIG. 5. *Error in the pressure (color) and the velocity (arrows) the MFMFE method (left) and the EMFE method (right) in Example 1. The two graphs are scaled differently. On the left, maximum pressure error (red) is 0.02 and maximum vector length is 0.21. On the right, maximum pressure error is 0.13 and maximum vector length is 9.35.*

The initial 8×8 mesh is generated from a square mesh by randomly perturbing the location of each vertex within a disk centered at the vertex with a radius $h\sqrt{2}/4$. The computed solution on the first level of refinement is shown in Figure 6. The numerical errors and convergence rates are obtained on a sequence of six mesh refinements and are reported in Table 2. As in the first example, the computationally obtained convergence rates for the MFMFE method confirm the theoretical results, while the EMFE method suffers a deterioration of accuracy along the non-smooth interfaces.

REMARK 4.1. We recently learned of the concurrent and related work of Klausen and Winther [14]. They formulate the MPFA method from [1] as a mixed finite element method using an enhanced Raviart-Thomas space and obtain convergence results on quadrilateral grids.

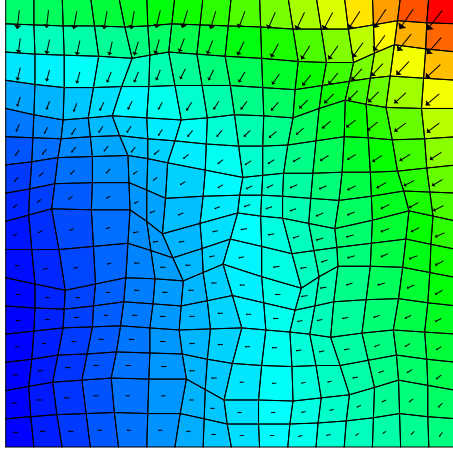


FIG. 6. Computed solution on the first level of refinement in Example 2.

TABLE 2
Discretization errors and convergence rates for Example 2.

$1/h$	MFMFEM			EMFE method	
	$\ p - p_h\ $	$\ \mathbf{u} - \mathbf{u}_h\ $	$\ \mathbf{u} - \mathbf{u}_h\ $	$\ p - p_h\ $	$\ \mathbf{u} - \mathbf{u}_h\ $
8	0.10E-1	0.85E-1	0.24E-1	0.19E-1	0.17E0
16	0.27E-2	0.55E-1	0.87E-2	0.88E-2	0.13E0
32	0.70E-3	0.30E-1	0.27E-2	0.45E-2	0.96E-1
64	0.18E-3	0.16E-1	0.73E-3	0.23E-2	0.69E-1
128	0.45E-4	0.81E-2	0.19E-3	0.12E-2	0.50E-1
256	0.11E-4	0.41E-2	0.50E-4	0.59E-3	0.35E-1
Rate	1.99	0.98	1.95	0.99	0.49

APPENDIX

A. Approximation properties of Π .LEMMA A.1. If E is a quadrilateral, then

$$\|\mathbf{q} - \Pi\mathbf{q}\|_E \leq C\|\mathbf{q}\|_{2,E}h^2. \quad (\text{A.1})$$

If E is an h^2 -quadrilateral, then

$$\|\mathbf{q} - \Pi\mathbf{q}\|_E \leq C\|\mathbf{q}\|_{2,E}h. \quad (\text{A.2})$$

If E is an h^2 -parallelogram, then

$$\|\nabla \cdot (\mathbf{q} - \Pi\mathbf{q})\|_E \leq C\|\nabla \cdot \mathbf{q}\|_{1,E}h. \quad (\text{A.3})$$

Proof. Bound (A.1) has been shown in [20]. The proof of (A.2) is a modification of the argument in [20]. Using Lemma 2.1, the definition of $\widehat{\mathbf{V}}(\widehat{E})$, and the Bramble-Hilbert lemma,

$$\|\mathbf{q} - \Pi\mathbf{q}\|_E \leq C\|\widehat{\mathbf{q}} - \widehat{\Pi}\widehat{\mathbf{q}}\|_{\widehat{E}} \leq C([\widehat{q}_1]_{2,\widehat{E},\widehat{y}} + [\widehat{q}_2]_{2,\widehat{E},\widehat{x}}), \quad (\text{A.4})$$

where $[\widehat{q}_1]_{2,\widehat{E},\widehat{y}} = \|\partial^2\widehat{q}_1/\partial\widehat{y}^2\|_{\widehat{E}}$ and $[\widehat{q}_2]_{2,\widehat{E},\widehat{x}} = \|\partial^2\widehat{q}_2/\partial\widehat{x}^2\|_{\widehat{E}}$. Letting $\mathbf{g} = \mathbf{r}_{21} - \mathbf{r}_{34}$, it is easy to see from (2.3) that

$$J_E DF_E^{-1} = A + \begin{bmatrix} g_2\widehat{x} & -g_1\widehat{x} \\ -g_2\widehat{y} & g_1\widehat{y} \end{bmatrix} + \bar{R}, \quad (\text{A.5})$$

where A is a constant matrix and $\|\bar{R}\|_{j,\infty,\widehat{E}} \leq Ch^2$, $j = 0, 1, 2$. Using that $\widehat{\mathbf{q}} = J_E DF_E^{-1}\tilde{\mathbf{q}}$, where $\tilde{\mathbf{q}}(\widehat{x}) = \mathbf{q} \circ F_E(\widehat{x})$, (A.4) and (A.5) imply

$$\|\mathbf{q} - \Pi\mathbf{q}\|_E \leq C(h([\tilde{q}_1]_{2,\widehat{E},\widehat{y}} + [\tilde{q}_2]_{2,\widehat{E},\widehat{x}}) + h^2\|\tilde{\mathbf{q}}\|_{2,\widehat{E}}),$$

where we have also used (2.6). Bound (A.2) now follows from a change of variables back to E .

To show (A.3) we first note that (2.11) and $(\nabla \cdot \mathbf{v}, w)_E = (\widehat{\nabla} \cdot \widehat{\mathbf{v}}, \widehat{w}J_E)_{\widehat{E}}$ imply

$$\nabla \cdot \mathbf{v} = \left(\frac{1}{J_E} \widehat{\nabla} \cdot \widehat{\mathbf{v}} \right) \circ F_E^{-1}(\mathbf{x}). \quad (\text{A.6})$$

The above relation gives

$$\int_E (\nabla \cdot (\mathbf{q} - \Pi\mathbf{q}))^2 dx = \int_{\widehat{E}} \frac{1}{J_E^2} (\widehat{\nabla} \cdot (\widehat{\mathbf{q}} - \widehat{\Pi}\widehat{\mathbf{q}}))^2 J_E d\widehat{\mathbf{x}} \leq Ch^{-2} |\widehat{\nabla} \cdot \widehat{\mathbf{q}}|_{1,\widehat{E}}^2, \quad (\text{A.7})$$

where we have used (2.6), (2.14), and the Bramble-Hilbert lemma for the inequality. On the other hand,

$$\begin{aligned} |\widehat{\nabla} \cdot \widehat{\mathbf{q}}|_{1,\widehat{E}} &= |J_E \widehat{\nabla} \cdot \widehat{\mathbf{q}}|_{1,\widehat{E}} \\ &\leq C(\|J_E\|_{\infty,\widehat{E}} |\widehat{\nabla} \cdot \widehat{\mathbf{q}}|_{1,\widehat{E}} + |J_E|_{1,\infty,\widehat{E}} \|\widehat{\nabla} \cdot \widehat{\mathbf{q}}\|_{\widehat{E}}) \\ &\leq C(h^2 |\widehat{\nabla} \cdot \widehat{\mathbf{q}}|_{1,\widehat{E}} + h^3 \|\widehat{\nabla} \cdot \widehat{\mathbf{q}}\|_{\widehat{E}}), \end{aligned} \quad (\text{A.8})$$

using (2.8) for the last inequality. Combining (A.7) – (A.8) and changing variables back to E implies (A.3). \square

REFERENCES

- [1] I. AAVATSMARK, *An introduction to multipoint flux approximations for quadrilateral grids*, Comput. Geosci., 6 (2002), pp. 405–432.
- [2] I. AAVATSMARK, T. BARKVE, Ø. BØE, AND T. MANNSETH, *Discretization on unstructured grids for inhomogeneous, anisotropic media. I. Derivation of the methods*, SIAM J. Sci. Comput., 19 (1998), pp. 1700–1716 (electronic).

- [3] T. ARBOGAST, C.N. DAWSON, P.T. KEENAN, M.F. WHEELER, AND I. YOTOV, *Enhanced cell-centered finite differences for elliptic equations on general geometry*, SIAM J. Sci. Comp., 19 (1998), pp. 404–425.
- [4] T. ARBOGAST, M.F. WHEELER, AND I. YOTOV, *Mixed finite elements for elliptic problems with tensor coefficients as cell-centered finite differences*, SIAM J. Numer. Anal., 34 (1997), pp. 828–852.
- [5] K. AZIZ AND A. SETTARI, *Petroleum reservoir simulation*, Applied Science Publishers, London and New York, 1979.
- [6] J. BARANGER, J.-F. MAITRE, AND F. OUDIN, *Connection between finite volume and mixed finite element methods*, RAIRO Modél. Math. Anal. Numér., 30 (1996), pp. 445–465.
- [7] F. BREZZI, J. DOUGLAS, JR., AND L.D. MARINI, *Two families of mixed elements for second order elliptic problems*, Numer. Math., 88 (1985), pp. 217–235.
- [8] F. BREZZI AND M. FORTIN, *Mixed and Hybrid Finite Element Methods*, vol. 15 of Springer Series in Computational Mathematics, Springer Verlag, Berlin, 1991.
- [9] Z. CAI, J.E. JONES, S.F. McCORMICK, AND T.F. RUSSELL, *Control-volume mixed finite element methods*, Comput. Geosci., 1 (1997), pp. 289–315 (1998).
- [10] P.G. CIARLET, *The finite element method for elliptic problems*, North-Holland, New York, 1978.
- [11] R.E. EWING, M. LIU, AND J. WANG, *Superconvergence of mixed finite element approximations over quadrilaterals*, SIAM J. Numer. Anal., 36 (1999), pp. 772–787.
- [12] J.M. HYMAN, M. SHASHKOV, AND S. STEINBERG, *The numerical solution of diffusion problems in strongly heterogeneous non-isotropic materials*, J. Comput. Phys., 132 (1997), pp. 130–148.
- [13] R.A. KLAUSEN AND T.F. RUSSELL, *Relationships among some locally conservative discretization methods which handle discontinuous coefficients*. To appear in Computational Geosciences.
- [14] R.A. KLAUSEN AND R. WINTHER, *Convergence of multi point flux approximations on quadrilateral grids*. Preprint.
- [15] S. MICHELETTI, R. SACCO, AND F. SALERI, *On some mixed finite element methods with numerical integration*, SIAM J. Sci. Comput., 23 (2001), pp. 245–270 (electronic).
- [16] R.A. RAVIART AND J.M. THOMAS, *A mixed finite element method for 2nd order elliptic problems*, in Mathematical Aspects of the Finite Element Method, Lecture Notes in Mathematics, vol. 606, Springer-Verlag, New York, 1977, pp. 292–315.
- [17] T.F. RUSSELL AND M.F. WHEELER, *Finite element and finite difference methods for continuous flows in porous media*, in The Mathematics of Reservoir Simulation, R. E. Ewing, ed., vol. 1 of Frontiers in Applied Mathematics, SIAM, Philadelphia, PA, 1983, pp. 35–106.
- [18] J.M. THOMAS, *Sur l'analyse numérique des méthodes d'éléments finis hybrides et mixtes*, PhD thesis, Université Pierre et Marie Curie, Paris, 1977.
- [19] P.S. VASSILEVSKI, S.I. PETROVA, AND R.D. LAZAROV, *Finite difference schemes on triangular cell-centered grids with local refinement*, SIAM J. Sci. Statist. Comput., 13 (1992), pp. 1287–1313.
- [20] J. WANG AND T.P. MATHEW, *Mixed finite element method over quadrilaterals*, in Conference on Advances in Numerical Methods and Applications, I. T. Dimov, B. Sendov, and P. Vassilevski, eds., World Scientific, River Edge, NJ, 1994, pp. 203–214.
- [21] A. WEISER AND M.F. WHEELER, *On convergence of block-centered finite-differences for elliptic problems*, SIAM J. Numer. Anal., 25 (1988), pp. 351–375.
- [22] M.F. WHEELER AND I. YOTOV, *A multipoint flux mixed finite element method*, Tech. Rep. TR Math 05-06, Dept. Math., University of Pittsburgh, 2005.